

A finite element model based on triangular mesh for convection-dominated stationary flows

Khouane Meftah*

IS2M Laboratory, Faculty of Technology, University of Abu Bekr Belkaid, Tlemcen, Algeria

The fluctuation distribution method is presented in this work to deal with the convection terms of the general transport equation. The fluctuation represents the convective surface exchange within an element. The solution method consists of defining numerical schemes to distribute this fluctuation. To that end, we introduce a new variable to rewrite the variational formulation with linear triangular element and weighted functions appropriately selected. The method is found to be accurate with minimum of dispersion or diffusion in the vicinity of the discontinuity. This method is interesting because there are no parameters to choose and can be an alternative to the famous streamline upwind Petrov–Galerkin method.

Keywords: FEM; convection dominated; stationary flows; triangular mesh

1. Introduction

The numerical treatment of the advection phenomenon is still attracting considerable research interest. Numerical analysts are constantly looking for more stable, accurate and efficient approximation of the advection terms in the general transport equation.

Initial attempts to deal with such terms using central difference operators in the finite difference method resulted in spurious oscillations for cases with grid Peclet number greater than 1. This shortcoming has been alleviated by the use of exponential and hybrid schemes (Spalding, 1972), the power-law scheme (Patankar, 1980), the higher order upwind differencing scheme (Atias, Wolfshtein, & Israeli, 1977; Sprice, Varga, & Warren, 1966), the quadratic upwind scheme (Leonard, 1979), streamline upwind scheme (Raithby, 1976) and total variation diminishing schemes (Harten, 1983; Le Veque Randall, 1992).

The finite element method (FEM) leads to similar difficulties. The conventional Galerkin weighted residual approach, similar to the central difference operator, produces acceptable levels of numerical diffusion and spatial oscillations.

To overcome these difficulties, two approaches have been adopted in the finite element model: a sort of upwind scheme based on streamline upwind Petrov–Galerkin (SUPG) formulation (Brooks & Hughes, 1980) and a higher order central scheme for temporal problems (Lax–Wendroff or Taylor–Galerkin scheme) (Lax & Wendroff, 1960; Meftah, 1998; Meftah & Dhath, 1996). The application of SUPG scheme requires an appropriate choice of stabilising coefficient, whereas Lax–Wendroff scheme is mainly adapted to temporal problems.

*Email: k_meftah@mail.univ-tlemcen.dz

In this paper, we develop a finite element model for convection-dominated stationary flows based on fluctuation distribution. This method has already been successfully applied to finite volume models for solving temporal scalar transport equation (Boulercha, 1993; Deconinck & Ricchiuto, 2007; Roe, 1982). In the present study, the same idea is used and applies it to the stationary transport equation and for a finite element model, but for a triangular mesh only.

2. Weak formulation of transport equation

A stationary transport equation involving convection and diffusion terms may be written as follows:

$$\vec{u}\vec{\nabla}c + \text{Div}\vec{q}_d - f = 0 \quad \text{on } A \quad (1a)$$

We introduce a new variable ϕ to rewrite the preceding equation as follows:

$$\begin{cases} \phi + \text{Div}\vec{q}_d - f = 0 & \text{on } A \\ \phi - \vec{u}\vec{\nabla}c = 0 \end{cases} \quad (1b)$$

$c = \bar{c}$ on S_1 and $\vec{q}_d\vec{n} = -f_s$ on S_2 .

where c is the scalar variable, for example concentration or temperature, etc. \vec{u} is the known velocity field and f is the source term. S_1 and S_2 represent the perimeter of A .

The diffusion term for isotropic case is:

$$\vec{q}_d = -\lambda\vec{\nabla}c \quad (2)$$

where λ is the diffusion coefficient.

A weak formulation associated with Equation (1b) is given as follows:

$$\begin{cases} W_k = W_c + W_d + W_f + W_S = 0 \\ W_\phi = 0 \end{cases} \quad (3a)$$

with:

$$W_c = \int_A \Psi_k \phi \, dA \quad (3b)$$

$$W_d = \int_A \vec{\nabla}\delta c \cdot \lambda\vec{\nabla}c \, dA \quad (3c)$$

$$W_f = - \int_A \delta c f \, dA \quad (3d)$$

$$W_S = - \int_{S_2} \delta c f_s \, ds \quad (3e)$$

$$W_\phi = \int_A \Psi_\phi (\phi - \vec{u} \nabla c) dA \quad (3f)$$

Ψ_k , δc and Ψ_ϕ are the test functions.

2.1. Finite element model

In this section, we present the formulation for a three-node triangular element (Figure 1).

For two-dimensional problems, the finite element representation becomes:

$$A = \sum A^e, \quad S_2 = \sum S^e \quad (4)$$

where A^e is the element geometry which is a three-noded triangle in our case. S^e is the length of the boundary element.

Equation (3a) becomes:

$$W_k = \sum_{A^e} \underbrace{(W_c^e + W_d^e)}_{W_k^e} + \sum_{A^e} W_f^e + \sum_{S^e} W_S^e = 0 \quad (5a)$$

$$W_\phi = \sum_{A^e} W_\phi^e = 0. \quad (5b)$$

The particularity of our flux distribution model is the choice of approximation functions for ϕ , c and related test functions Ψ_ϕ , δc and Ψ_k .

c and δc are represented by classical C^0 approximation for each element.

$$c = \sum N_i c_i, \quad \delta c = \sum N_i \delta c_i \quad (6)$$

$$N_1 = 1 - \xi - \eta, \quad N_2 = \xi, \quad N_3 = \eta \quad (7)$$

ϕ and Ψ_ϕ are local and constant over each element.

$$\phi = \phi^e, \quad \Psi_\phi = 1 \quad (8)$$

Using Equations (3f) and (5b), we obtain:

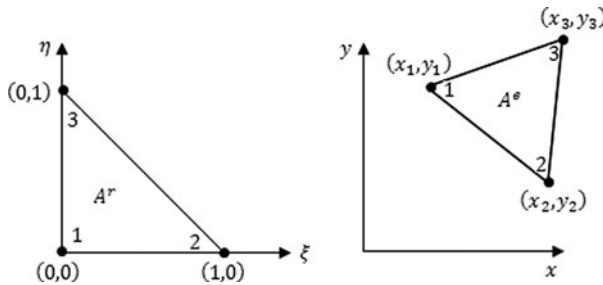


Figure 1. Triangular element (reference element, real element).

$$\phi^e = \frac{1}{A^e} \int_{A^e} \vec{u} \vec{\nabla} c \, dA \quad (9)$$

The Jacobian $[J]$ is defined by:

$$[J] = \begin{bmatrix} x_2 - x_1 & y_2 - y_1 \\ x_3 - x_1 & y_3 - y_1 \end{bmatrix} \quad (10)$$

$$\vec{\nabla}_{(x,y)} c = [j] \vec{\nabla}_{(\xi,\eta)} c = \frac{1}{2A^e} \sum_{i=1}^3 \{n_i\} c_i \quad (11)$$

$$[j] = [J]^{-1}, \quad A^e = \frac{1}{2} \det([J]) \quad (12)$$

$$\{n_1\} = \begin{Bmatrix} -(y_3 - y_2) \\ x_3 - x_2 \end{Bmatrix}, \quad \{n_2\} = \begin{Bmatrix} -(y_1 - y_3) \\ x_1 - x_3 \end{Bmatrix}, \quad \{n_3\} = \begin{Bmatrix} -(y_2 - y_1) \\ x_2 - x_1 \end{Bmatrix} \quad (13)$$

Note that:

$$\{n_1\} + \{n_2\} + \{n_3\} = 0 \quad (14)$$

The normal vectors \vec{n}_1 , \vec{n}_2 and \vec{n}_3 are shown in Figure 2.

Using Equations (9) and (11), we obtain:

$$\phi^e = \frac{1}{A^e} \sum_{i=1}^3 k_i c_i = \frac{1}{A^e} \langle k_1 \quad k_2 \quad k_3 \rangle \begin{Bmatrix} c_1 \\ c_2 \\ c_3 \end{Bmatrix} \quad (15)$$

with:

$$k_i = \frac{1}{2} \vec{u} \cdot \vec{n}_i \quad (16)$$

Using Equation (14), we obtain:

$$\sum_{i=1}^3 k_i = 0 \quad (17)$$

The flux distribution model is related to the choice of the test functions Ψ_k .

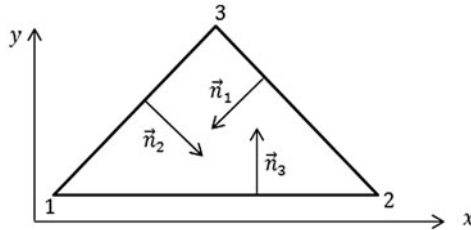


Figure 2. Illustration of the normal vectors.

$$\Psi_k = \sum_{i=1}^3 P_i^k \delta c_i \quad (18)$$

For conservation, we should have:

$$\sum_{i=1}^3 P_i^k = 1, \quad \sum_{i=1}^3 N_i = 1 \quad (19)$$

For each triangular element, we have:

$$W_k^e = \langle \delta c_1 \ \delta c_2 \ \delta c_3 \rangle ([k_c^e] + [k_d^e]) \begin{Bmatrix} c_1 \\ c_2 \\ c_3 \end{Bmatrix} \quad (20)$$

$$W_f^e = \langle \delta c_1 \ \delta c_2 \ \delta c_3 \rangle \{f^e\} \quad (21)$$

Using Equations (3c) and (11), we obtain:

$$[k_d^e] = \frac{\lambda}{4A^e} B^T B \quad (22)$$

$$B = [\{n_1\} \{n_2\} \{n_3\}] \quad (23)$$

$$\{f^e\} = -\frac{A^e}{3} f \begin{Bmatrix} 1 \\ 1 \\ 1 \end{Bmatrix} \quad (24)$$

Using Equations (15) and (18), we obtain:

$$[k_c^e] = \{a\} \langle k_1 \ k_2 \ k_3 \rangle \quad (25)$$

with:

$$\{a\} = \frac{1}{A^e} \int_{A^e} \{P^k\} dA \quad (26)$$

For each boundary element, we have:

$$W_S^e = \langle \delta c_1 \ \delta c_2 \rangle \{r^e\} \quad (27)$$

$$\{r^e\} = -\frac{S_e}{2} f_s \begin{Bmatrix} 1 \\ 1 \end{Bmatrix} \quad (28)$$

2.2. Construction of $\{a\}$

The test functions P_i^k are chosen in a particular way depending on the nature of velocity field assumed constant over each element. For a given triangle, the velocity field may lead to the following two situations:

2.2.1. Inflow restricted to one side of the element

The flux enters from one side and exits from the two remaining sides.

In the case of inflow restricted to one side of the element (Figure 3), $k_1 > 0$, $k_2 < 0$, $k_3 < 0$, all the flow is restricted to go through side (1). We take in this case:

$$P_1^k = 1, P_2^k = 0, P_3^k = 0 \tag{29}$$

Equation (26) becomes:

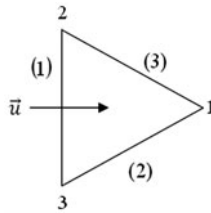


Figure 3. Inflow restricted to one side of the element.

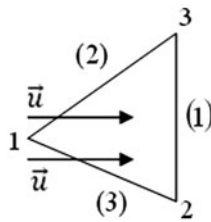


Figure 4. Inflow through two sides of the element.

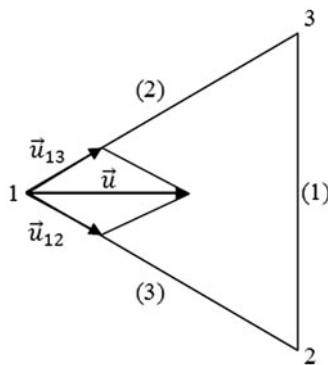


Figure 5. N scheme.

$$\{a\} = \begin{Bmatrix} 1 \\ 0 \\ 0 \end{Bmatrix} \quad (30)$$

Using Equation (25), we obtain:

$$[k_c^e] = \begin{bmatrix} k_1 & k_2 & k_3 \\ 0 & 0 & 0 \\ 0 & 0 & 0 \end{bmatrix} \quad (31)$$

2.2.2. Inflow through two sides of the element

The flux enters from two sides and exits from the remaining side.

In the case of inflow through two sides of the element (Figure 4), $k_1 < 0$, $k_2 > 0$, $k_3 > 0$ several schemes are considered.

(a) *N scheme*

We project the velocity along sides (2) and (3) as shown in Figure 5.

$$\vec{u} = \vec{u}_{12} + \vec{u}_{13}. \quad (32)$$

Therefore, the fluctuation is decomposed into two parts:

$$\phi^e = \phi_{12} + \phi_{13} \quad (33)$$

For component \vec{u}_{12} , we have $k_1 < 0$, $k_2 > 0$, $k_3 = 0$ and consequently the flow is restricted to go through side (2). Hence:

$$P_1^k = 0, P_2^k = 1, P_3^k = 0 \quad (34)$$

Equation (26) becomes:

$$\{a\} = \begin{Bmatrix} 0 \\ 1 \\ 0 \end{Bmatrix} \quad (35)$$

Using Equations (15) and (17), we obtain:

$$\phi_{12} = \frac{1}{A^e} \langle k_1 \ k_2 \ k_3 \rangle \begin{Bmatrix} c_1 \\ c_2 \\ c_3 \end{Bmatrix} = \frac{1}{A^e} \langle -k_2 \ k_2 \ 0 \rangle \begin{Bmatrix} c_1 \\ c_2 \\ c_3 \end{Bmatrix} \quad (36)$$

For component \vec{u}_{13} , we have $k_1 < 0$, $k_2 = 0$, $k_3 > 0$ and therefore the flow is restricted to go through side (3). Hence:

$$P_1^k = 0, P_2^k = 0, P_3^k = 1 \quad (37)$$

Equation (26) becomes:

$$\{a\} = \begin{Bmatrix} 0 \\ 0 \\ 1 \end{Bmatrix} \quad (38)$$

Using Equations (15) and (17), we have:

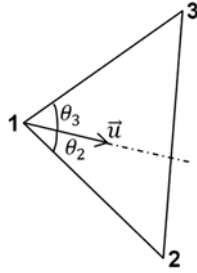


Figure 6. LDB scheme.

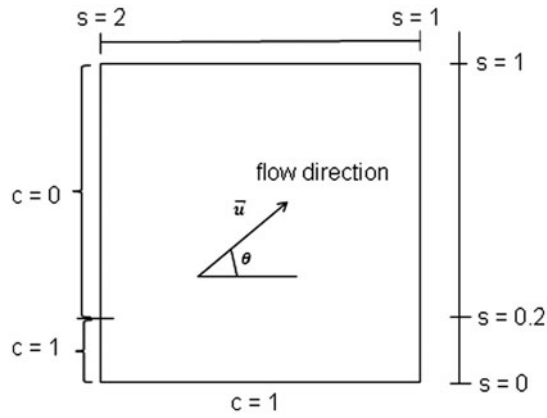


Figure 7. Advection skew to mesh.

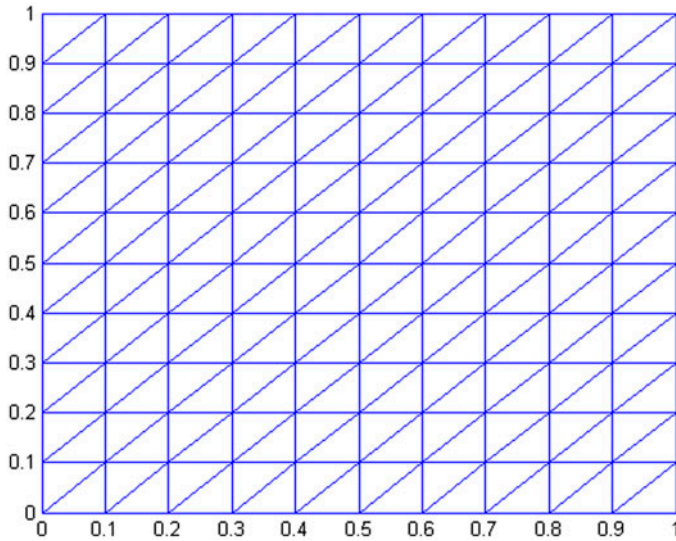


Figure 8. Computational grid for advection skew to mesh ($h = .1$).

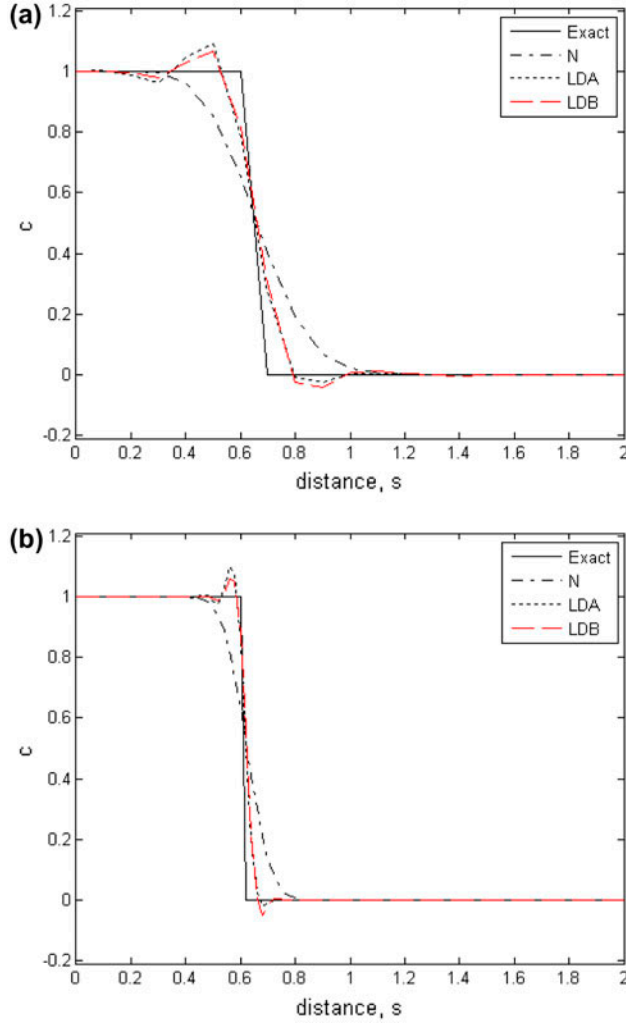


Figure 9. Variation of c along s , at flow angle $\theta = 22.5^\circ$, (a) $h = .1$ and (b) $h = .05$.

$$\phi_{13} = \frac{1}{A^e} \langle k_1 \ k_2 \ k_3 \rangle \begin{Bmatrix} c_1 \\ c_2 \\ c_3 \end{Bmatrix} = \frac{1}{A^e} \langle -k_3 \ 0 \ k_3 \rangle \begin{Bmatrix} c_1 \\ c_2 \\ c_3 \end{Bmatrix} \quad (39)$$

According to the Equation (33), we obtain:

$$[k_c^e] = \begin{Bmatrix} 0 \\ 1 \\ 0 \end{Bmatrix} - \langle k_2 \ k_2 \ 0 \rangle + \begin{Bmatrix} 0 \\ 0 \\ 1 \end{Bmatrix} \langle -k_3 \ 0 \ k_3 \rangle \quad (40)$$

$$[k_c^e] = \begin{bmatrix} 0 & 0 & 0 \\ -k_2 & k_2 & 0 \\ -k_3 & 0 & k_3 \end{bmatrix} \quad (41)$$

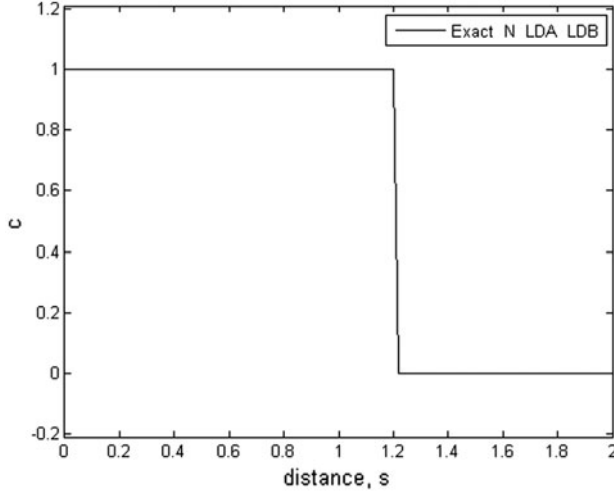


Figure 10. Variation of c along s , at flow angle $\theta = 45^\circ$ ($h = .1$ or $h = .05$).

(b) *LDA scheme*

The fluctuation is also decomposed into two parts as follows:

$$\phi_{12} = \alpha_2 \phi^e, \quad \phi_{13} = \alpha_3 \phi^e \quad (42)$$

$$\alpha_2 = -\frac{k_2}{k_1}, \quad \alpha_3 = -\frac{k_3}{k_1} \quad (43)$$

In this scheme, we assume:

$$P_1^k = 0, \quad P_2^k = \alpha_2, \quad P_3^k = \alpha_3 \quad (44)$$

Equation (26) becomes:

$$\{a\} = \begin{Bmatrix} 0 \\ \alpha_2 \\ \alpha_3 \end{Bmatrix} \quad (45)$$

According to Equation (25), we obtain:

$$[k_c^e] = \begin{bmatrix} 0 & 0 & 0 \\ \alpha_2 k_1 & \alpha_2 k_2 & \alpha_2 k_3 \\ \alpha_3 k_1 & \alpha_3 k_2 & \alpha_3 k_3 \end{bmatrix} \quad (46)$$

(c) *LDB scheme*

This scheme is similar to the previous scheme. The coefficients α_2 and α_3 are given as follows:

$$\alpha_2 = \frac{\cos\theta_2 \sin\theta_3}{\sin(\theta_2 + \theta_3)}, \quad \alpha_3 = \frac{\sin\theta_2 \cos\theta_3}{\sin(\theta_2 + \theta_3)} \quad (47)$$

θ_2 and θ_3 are shown in Figure 6.

$$\theta_2 = \frac{\pi}{2} - \text{Arccos} \left(\frac{2k_3}{|\vec{u}||\vec{n}_3|} \right), \quad \theta_3 = \frac{\pi}{2} - \text{Arccos} \left(\frac{2k_2}{|\vec{u}||\vec{n}_2|} \right) \quad (48)$$

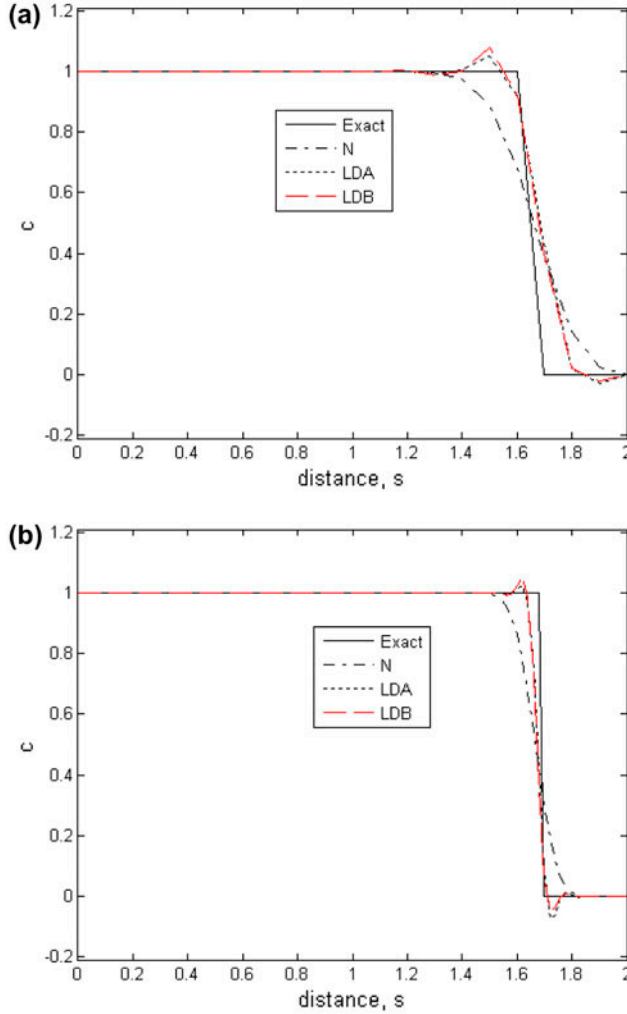


Figure 11. Variation of c along s , at flow angle $\theta = 67.5^\circ$, (a) $h = .1$ and (b) $h = .05$.

Algorithm

1. Compute $[k_c^e]$
 - a. Inflow restricted to one side of the element: $[k_c^e]$ is given by Equation (31)
 - b. Inflow through two sides of the element:
 - N scheme : $[k_c^e]$ is given by Equation (41)
 - LDA scheme : $[k_c^e]$ is given by Equations (43), (46)
 - LDB scheme : $[k_c^e]$ is given by Equations (47), (46)
2. Compute $[k_d^e]$ Equation (22)
3. Compute $\{f^e\}$ and $\{r^e\}$ Equations (24), (28)
4. Assemble matrices and solve

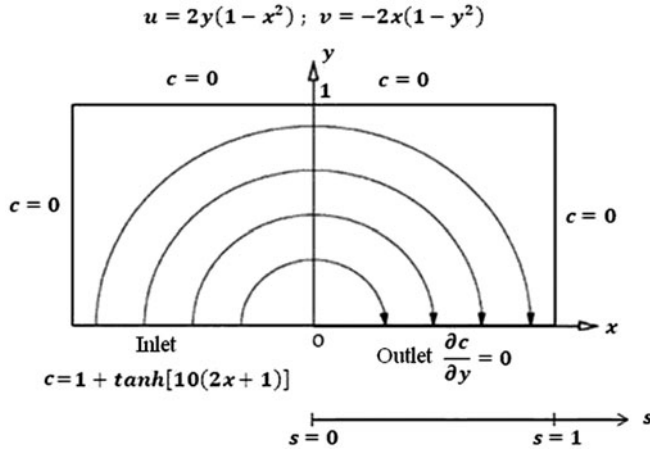


Figure 12. Schematic of the Smith–Hutton problem.

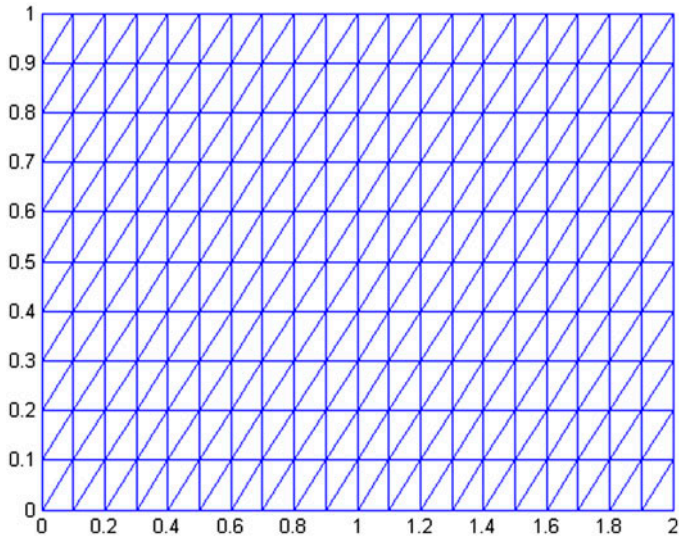


Figure 13. Computational grid for Smith–Hutton problem ($h = .1$).

3. Test case results

3.1. Advection skew to mesh

This test case has been commonly used to examine potential techniques to deal with the advection terms. The flow domain and the boundary conditions are shown in Figure 7.

The variation of c along the distance s is investigated for the case of pure advection ($\lambda = 0$) and for three flow angles $\theta = 22.5^\circ$, $\theta = 45^\circ$, $\theta = 67.5^\circ$. The distance s ($0 \leq s \leq 2$) is defined in Figure 7.

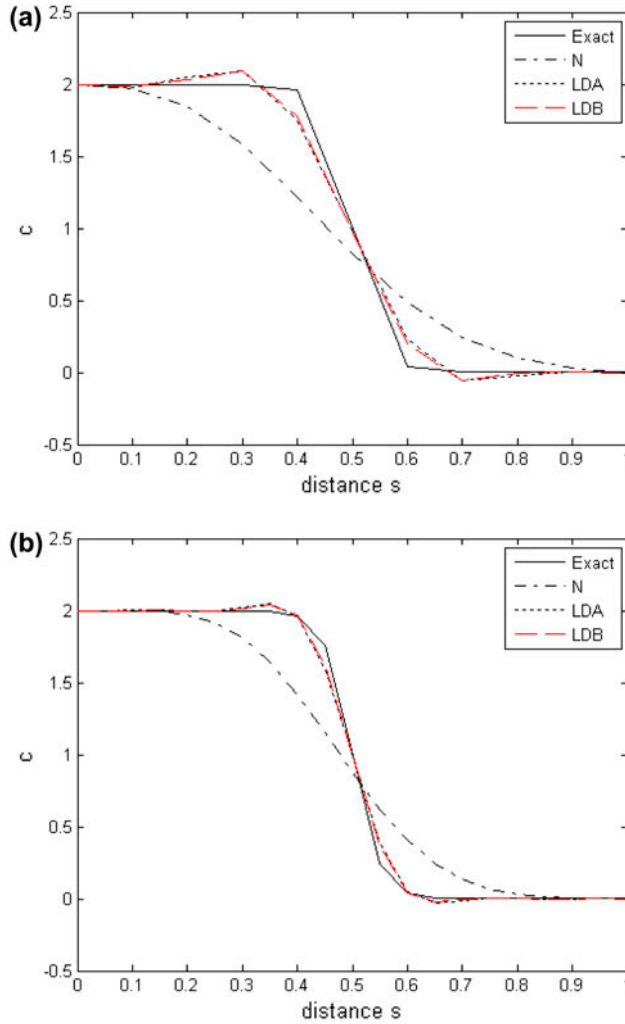


Figure 14. Variation of c along s for Smith and Hutton problem, (a) $h = .1$ and (b) $h = .05$.

As shown in Figure 8, the domain is subdivided into equally spaced rows and columns, resulting in a regular mesh ($\Delta x = \Delta y = h$).

Figures 9–11 show the results of the current work compared to the exact solution at flow angles $\theta = 22.5^\circ$, $\theta = 45^\circ$, $\theta = 67.5^\circ$ for two grids ($h = .1$ and $h = .05$).

For $\theta = 45^\circ$, all the schemes reproduce the exact solution. The fact that the schemes perform so well for an inflow direction of 45° is likely to be due to the fact that the inflow happens to be perfectly aligned with one of the sides of the triangle element in the mesh.

For $\theta = 22.5^\circ$ or 67.5° , the LDA and LDB schemes still give very good results, although they exhibit small oscillations when passing the discontinuity. The N scheme does not present any oscillations, however, it gives rise to diffusion.

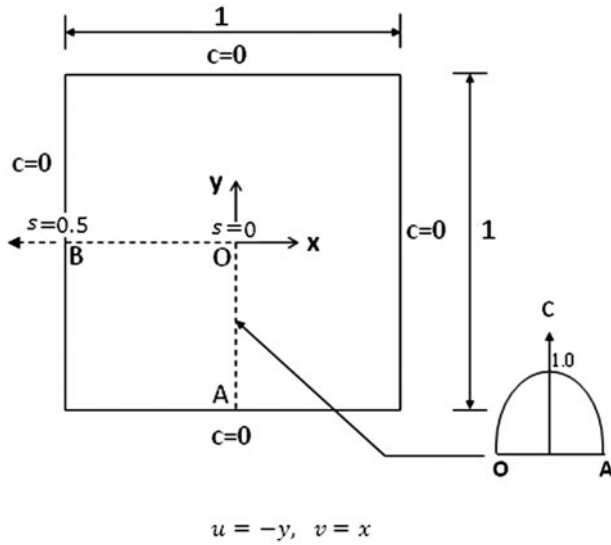


Figure 15. Rotating disc.

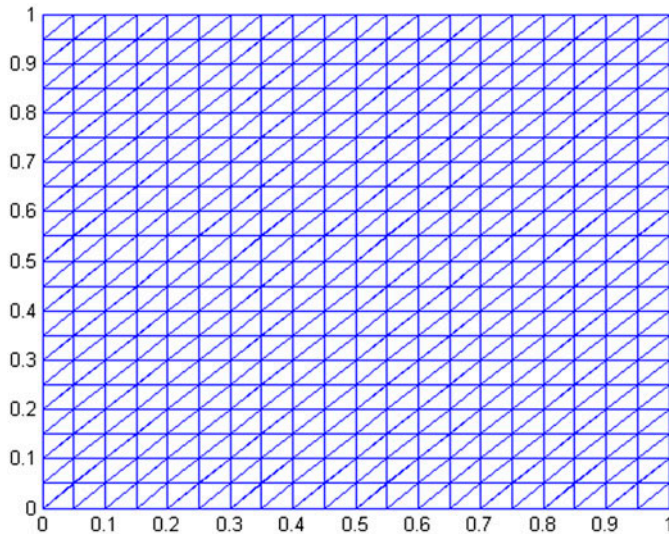


Figure 16. Computational grid for rotating disc ($h = .05$).

3.2. Smith and Hutton test case

This case was proposed by Smith and Hutton (1982). The flow domain and the boundary conditions are shown in Figure 12. As shown in Figure 13, the domain is subdivided into equally spaced rows and columns, resulting in a regular mesh ($\Delta x = \Delta y = h$). The variation of c along the distance s is investigated for the case of pure advection. s is the distance from the origin at the outlet ($0 \leq s \leq 1$) and is shown in Figure 12.

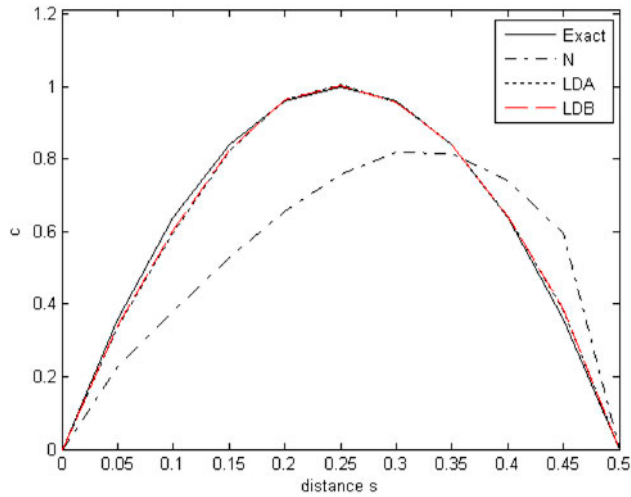


Figure 17. Variation of c along line OB for $h = .05$.

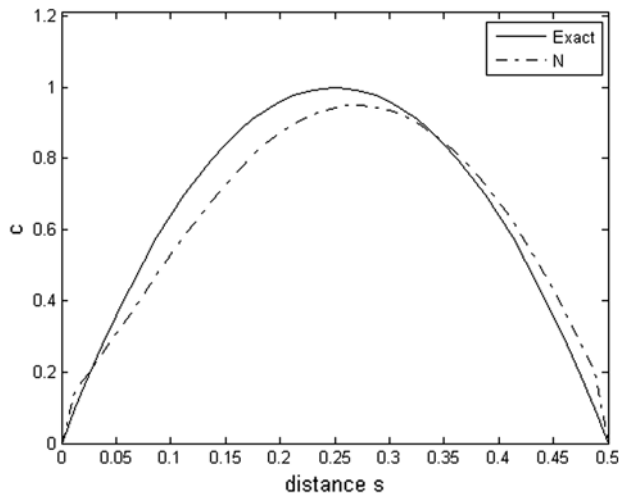


Figure 18. Variation of c along line OB for $h = .0125$.

Figure 14(a) and (b) shows the results of the current work compared to the exact solution for two grids ($h = .1$ and $h = .05$).

3.3. Rotating disc

The flow field and boundary conditions are depicted in Figure 15. It is assumed that c has a parabolic variation along OA and undisturbed around the square.

As shown in Figure 16, the domain is subdivided into 21 equally spaced rows and columns ($h = \Delta x = \Delta y = .05$), producing 441 nodes and 800 elements.

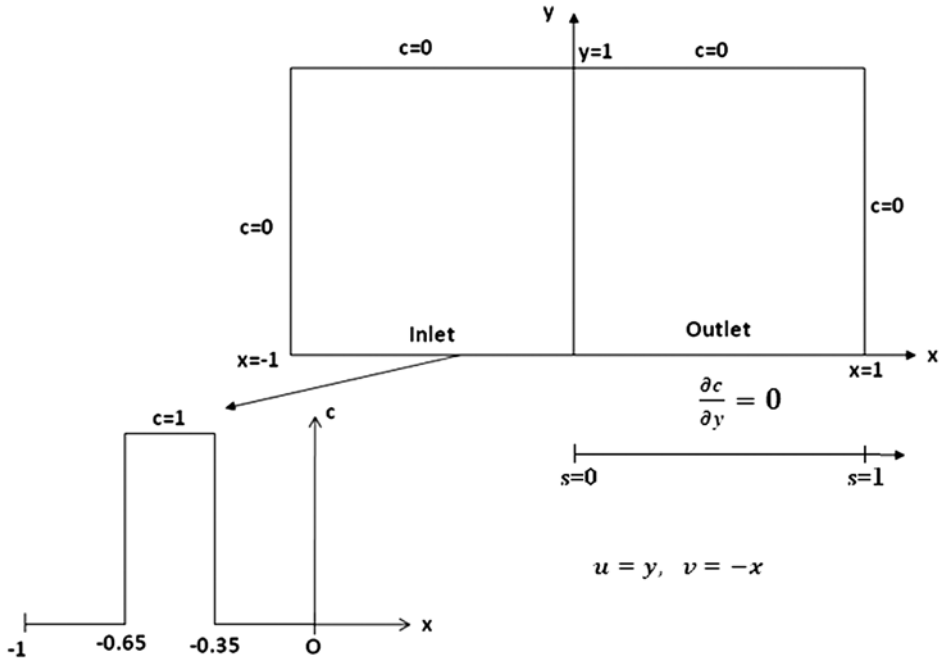


Figure 19. Rotation of a square profile.

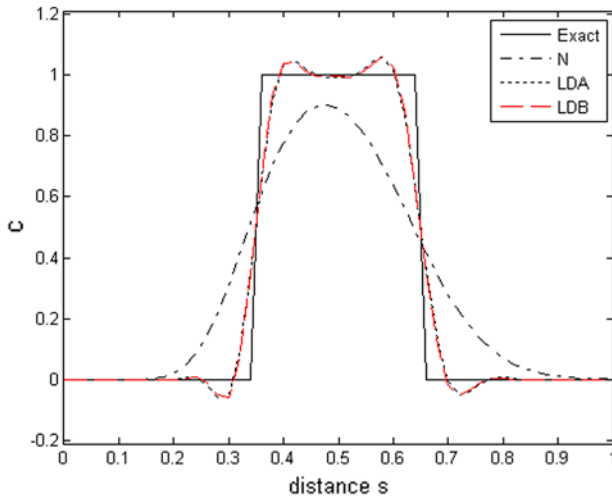


Figure 20. Variation of c along s .

The variation of c along the distance $s(0 \leq s \leq .5)$ is investigated for the case of pure advection. s is the distance along line OB (see Figure 15).

Figure 17 shows the results of the current work compared to the exact solution for $h = .05$. The LDA and LDB schemes lead to the exact solution. However, the N scheme gives the worse results that are shifted to the right. Nevertheless, for a finer mesh ($h = .0125$), the results become acceptable (see Figure 18).

3.4. Rotation of a square profile

The geometry, the physical properties and the boundary conditions are shown in Figure 19. We impose a square profile (of a highly nonlinear shape) on the inlet and we examine the variation of c along s , where s ($0 \leq s \leq 1$) is the distance from the origin at the outlet (see Figure 19).

The flow domain was divided into 101 rows and 51 columns ($h = \Delta x = \Delta y = .02$).

Figure 20 compares the results of the current work with the exact solution. The LDA and LDB schemes lead to good results and exhibit only small oscillations. The N scheme does not present any oscillations. However, it gives rise to diffusion.

4. Conclusion

The SUPG method is the only method to solve the convection-dominated stationary flows by FEM. This method is robust, but unfortunately requires an appropriate choice of stabilising coefficient. In this paper, we proposed another finite element model. Three schemes for a three-noded triangular element are presented: N scheme, LDA and LDB schemes. LDA and LDB schemes were proven to be very accurate; they generate small spurious oscillations in the vicinity of the discontinuity. The N scheme does not exhibit any oscillation, but unfortunately produces a numerical diffusion. The present method is very easy to implement and does not require a stabilisation term. This model can be an alternative to the famous SUPG model.

Disclosure statement

No potential conflict of interest was reported by the author.

References

- Atias, M., Wolfshtein, M., & Israeli, M. (1977). Efficiency of Navier–Stokes solvers. *AIAA Journal*, *15*, 263–266.
- Boulercha, M. (1993). *Ecoulement eulériens par éléments finis avec raffinement du maillage* [Finite element modeling of eulerian flows with mesh refinement] (PhD thesis). Université Laval, Québec.
- Brooks, A. N., & Hughes, T. J. (1980). Streamline upwind Petrov–Galerkin methods for advection dominated flows. *Proceedings of the Third International Conference on Finite Element Methods in Fluid Flow*, Banff.
- Deconinck, H., & Ricchiuto, M. (2007). Residual distribution schemes: Foundations and analysis. In E. Stein, E. de Borst, & T. J. Hughes (Eds.), *Encyclopedia of computational mechanics, volume 3: Fluids*. Chichester: Wiley.
- Harten, A. (1983). High resolution schemes for hyperbolic conservation laws. *Journal of Computational Physics*, *49*, 357–393.
- Lax, P. D., & Wendroff, B. (1960). Systems of conservation laws. *Communications on Pure and Applied Mathematics*, *13*, 217–237.
- Leonard, B. P. (1979). A stable and accurate convective modeling procedure based on quadratic upstream interpolation. *Computer Methods in Applied Mechanics and Engineering*, *19*, 59–98.
- Le Veque Randall, J. (1992). *Numerical methods for conservation laws. Lectures in Mathematics, ETH Zurich*. Zurich: Birkhäuser Verlag.
- Meftah, K. (1998). *Modélisation tridimensionnelle de l'hydrodynamique et du transport par suspension* [Three-dimensional modeling of hydrodynamics and transport suspension] (PhD thesis). Université de Technologie de Compiègne, France.

- Meftah, K., & Dhatt, G. (1996, Mars). *Schémas centrés et décentrés en convection-diffusion* [Centered and decentered schemes for convection-diffusion problems]. Congrès Magrébin Ghardaia [Physics Maghreb Conference], Ghardaia, Algeria.
- Patankar, S. V. (1980). *Numerical heat transfer and fluid flow*. New York, NY: Hemisphere/MC Graw-Hill.
- Raithby, G. S. (1976). Skew upstream differencing schemes for problems involving fluid flow. *Computer Methods in Applied Mechanics and Engineering*, 9, 153–164.
- Roe, P. L. (1982). Fluctuations and signals – A framework for numerical evolution problems. In K. W. Morton & M. J. Baines (Eds.), *Numerical methods for fluid dynamics* (pp. 219–257). London: Academic Press.
- Smith, R. M., & Hutton, A. G. (1982). The numerical treatment of advection: A performance comparison of current methods. *Numerical Heat Transfer*, 5, 439–461.
- Spalding, D. (1972). A novel finite difference formulation for differential expressions involving both first and second derivatives. *International Journal for Numerical Methods in Engineering*, 4, 551–559.
- Spruce, H., Varga, R. S., & Warren, J. E. (1966). Application of oscillations matrices to diffusion – correction equations. *Journal of Mathematical Physics*, 45, 301–311.